Lattice Kinetic Theory in a Comoving Galilean Reference Frame

N. Frapolli,* S. S. Chikatamarla,† and I. V. Karlin‡
Department of Mechanical and Process Engineering, ETH Zurich, 8092 Zurich, Switzerland
(Received 25 April 2016; published 30 June 2016)

We prove that the fully discrete lattice Boltzmann method is invariant with respect to Galilean transformation. Based on this finding, a novel class of shifted lattices is proposed which dramatically increases the operating range of lattice Boltzmann simulations, in particular, for gas dynamics applications. A simulation of vortex-shock interaction is used to demonstrate the accuracy and efficiency of the proposed lattices. With one single algorithm it is now possible to simulate a broad range of applications, from low Mach number flows to transonic and supersonic flow regimes.

DOI: 10.1103/PhysRevLett.117.010604

The lattice Boltzmann (LB) method [1–5] is a modern approach to the simulation of complex flows such as turbulence [6], surface and multiphase phenomena [7–11], microemulsions and soft-glassy materials [12], relativistic hydrodynamics [13], hemodynamics [14], and *ab initio* electronic structure calculations [15]. The LB method is a recast of the continuum fluid mechanics in a form of a fully discrete kinetic equation for the populations of designer particles $f_i(\boldsymbol{x},t)$, with the simplest rule of propagation on a space-filling lattice formed by discrete velocities $\boldsymbol{v}_i$, $i=1,\ldots,Q$, in discrete-time steps, and relaxation at the nodes $\boldsymbol{x}$ to a local equilibrium $f_i^{\mathrm{eq}}(\boldsymbol{x},t)$. As an indicator example, we write a typical LB equation:

$$f_i(\boldsymbol{x}+\boldsymbol{v}_i,t+1)=f_i(\boldsymbol{x},t)+\omega\big(f_i^{\mathrm{eq}}(\boldsymbol{x},t)-f_i(\boldsymbol{x},t)\big), \quad (1)$$

where the propagation is on the left and postrelaxation is on the right, while the relaxation parameter ω encodes transport coefficients.

However, existing LB models violate the basic physical requirement of Galilean frame indifference. This violation manifests itself in the use of *symmetric* lattices, which amounts to fixing a preferred reference frame "at rest." While symmetric lattices work well for incompressible flows, they are quite restrictive when the flow speed approaches the speed of sound [16–21]. For example, in the case of a shock wave traveling at a speed U relative to a laboratory reference frame, the physics of the problem clearly prefers the comoving reference frame. So, the question arises: Is LB bound to the once chosen, traditional reference frame at rest, or is there a way to formulate LB in other Galilean reference frames? This question is all but academic, as incompressible and compressible flows are fundamentally different [22], with turbulence on one end and shock waves on the other. The difficulty in bridging these two limits is well recognized in the conventional fluid dynamics [23,24]: Simulation of compressible flows requires dissipation to stabilize shocks, while accurate results for turbulence are achieved with low numerical dissipation. Thus, a single LB algorithm with the propagation Eq. (1) for both high and low Mach numbers is highly desirable.

Here we prove that the LB method stays invariant in any Galilean reference frame. The proof is based on a simple observation about the Galilean invariance of the lattice equilibrium distribution. Based on that, we introduce *shifted* lattices (see the example in Fig. 1) which, nonetheless, are realized with the standard propagation-collision algorithm Eq. (1), on the same grids and with the same boundary conditions as in the familiar symmetric case. We demonstrate a dramatic increase in operation capabilities of these shifted lattices by a complex vortex-shock interaction benchmark.

We begin with a brief summary on the LB models in the reference frame at rest [25–27]. Using the nomenclature $DdQn^d$ for a lattice with $Q=n^d$ speeds in $D=d$ spatial dimensions, the hierarchy of lattices is constructed as tensor products of D copies of one-dimensional symmetric velocity sets V_n. We shall consider $V_7=\{-3,-2,-1,0,1,2,3\}$ below as an example of the supersonic lattice Boltzmann simulation. For each velocity $v_i\in V_n$, one specifies a weight $W_i(0,T)$. To that end, consider the Maxwellian at unit density:

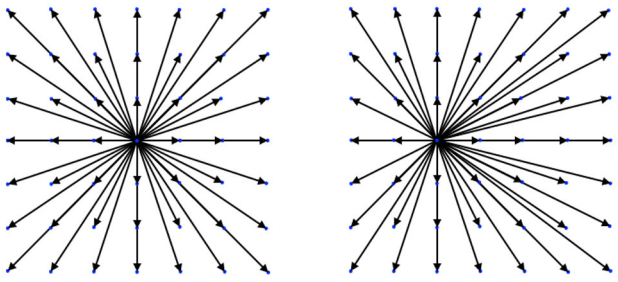

FIG. 1. Discrete velocities in two Galilean reference frames. Left: Symmetric lattice, standard reference frame ($U_x=0$, $U_y=0$). Right: Shifted lattice, comoving reference frame ($U_x=1$, $U_y=0$).

$$f_v^M(U,T) = \sqrt{\frac{1}{2\pi T}}\exp\left(-\frac{(v-U)^2}{2T}\right). \quad (2)$$

The weights for symmetric sets are found by matching the moments of the Maxwellian Eq. (2) at $U = 0$, $f_v^M(0,T)$. This reduces to a linear $n \times n$ algebraic system to be solved for the weights ($m = 0, \ldots, n-1$):

$$\langle W_i(0,T) v_i^m \rangle = \langle f_v^M(0,T) v^m \rangle, \quad (3)$$

where the operator $\langle \cdots \rangle$ stands for summation over discrete velocity index i for the discrete case (left) or integration over the continuous velocity v (right). In particular, for the velocity set V_7 the weights are $W_0(0,T) = (36 - 49T + 42T^2 - 15T^3)/36$, $W_{\pm1}(0,T) = T(12 - 13T + 5T^2)/16$, $W_{\pm2}(0,T) = T(-3 + 10T - 5T^2)/40$, and $W_{\pm3}(0,T) = T(4 - 15T + 15T^2)/720$. Once the weights are specified, the rest follows: For the symmetric lattice $D3Qn^3$, the weight of each discrete velocity $\boldsymbol{v}_i$ is the algebraic product of the one-dimensional weights corresponding to the projection of $\boldsymbol{v}_i$ onto the natural Cartesian directions, $W_i = W_{ix} W_{iy} W_{iz}$, where $W_{i\alpha}$ is the one-dimensional weight of $v_{i\alpha} \in V_n$. The weights uniquely specify the entropy function [28],

$$H = \langle f_i \ln (f_i / W_i) \rangle, \quad (4)$$

while the equilibrium is defined as a minimizer thereof under the constraints of local density $\rho = \langle f_i \rangle$, momentum $\rho \boldsymbol{u} = \langle f_i \boldsymbol{v}_i \rangle$, and energy $\rho(DT + u^2) = \langle f_i v_i^2 \rangle$. While the minimization may be done in various ways (exact solution in some cases, expansion of Lagrange multipliers, or direct numerical minimization), we stress that the weights defining the entropy function Eq. (4) is key. Moreover, we note that the accuracy of the resulting LB model is always limited by the finiteness of the primary one-dimensional velocity set V_n: Once the temperature T deviates too far from the reference temperature T_0 and/or the magnitude of the local flow velocity u deviates away from $u = 0$, the moments of the LB equilibrium drift away from the corresponding moments of the local Maxwellian. The reference temperature is the point at which the deviations are minimal; it is known for any admissible set V_n; cf. Refs. [25–27]. This is a significant drawback as it requires unduly large sets V_n to reach high Mach number flow regimes. Clearly, the origin of this is the choice of the preferred reference frame $U = 0$ at the outset. We wish to challenge the notion of a reference frame at rest; instead, we prefer to define the equilibrium in a frame moving, say, with the velocity U in the x direction. This is achieved by considering a *shifted* discrete velocity set V_n' with the velocities

$$v_i' = v_i + U, \qquad v_i \in V_n, \quad (5)$$

and finding the shifted weights $W_i(U,T)$ by matching the moments of the Maxwellian $f_v^M(U,T)$ (2). Instead of Eq. (3), we thus have

$$\langle W_i(U,T)[v_i + U]^m \rangle = \langle f_v^M(U,T) v^m \rangle. \quad (6)$$

The key observation is that the weights $W_i(U,T)$ are Galilean invariant: For any set V_n and for any shift U, we have

$$W_i(U,T) = W_i(0,T). \quad (7)$$

The proof of Eq. (7) follows immediately from Galilean invariance of the moments of the Maxwellian: Using the binomial theorem and Eq. (3), we write for $m = 0, \ldots, n-1$,

$$\begin{aligned}\langle f_v^M(U,T) v^m \rangle &= \sum_{k=0}^{m} \binom{m}{k} U^k \langle f_v^M(0,T) v^{m-k} \rangle \\ &= \sum_{k=0}^{m} \binom{m}{k} U^k \langle W_i(0,T) v_i^{m-k} \rangle \\ &= \langle W_i(0,T)[v_i + U]^m \rangle.\end{aligned}$$

Hence, Eq. (6) is equivalent to

$$\langle [W_i(U,T) - W_i(0,T)][v_i + U]^m \rangle = 0. \quad (8)$$

Since the shift U is arbitrary, the result Eq. (7) follows.

Galilean invariance of the weights Eq. (7) has a number of immediate important implications. First, the construction of the discrete velocities through tensor products in higher dimensions remains as before. For example, in two dimensions, the shift U in the x direction corresponds to the tensor product $V_{nx}' \otimes V_{ny}$. We shall use this example below. Second, the symmetric velocity sets generate space-filling lattices. This is crucial for the realization of the time-marching LB scheme Eq. (1). Now, if the shift U is itself integer, the corresponding shifted lattice is also space filling. For example, with $U = 1$, the shifted set V_7' becomes $V_7' = \{-2, -1, 0, 1, 2, 3, 4\}$. The shifted and the symmetric lattices, with the discrete velocities $V_{7x}' \otimes V_{7y}$ and $V_{7x} \otimes V_{7y}$, respectively, are shown in Fig. 1. Next, the weights corresponding to the velocities of the shifted lattice are the same as for the symmetric case: $W_i(U,T) = W_{ix}(0,T) W_{iy}(0,T)$. Moreover, since the weights do not change under a transform to a comoving reference frame, the entropy function is Galilean invariant, and is given by Eq. (4). Consequently, the equilibrium populations are form invariant. They are found by the same minimization techniques as in the familiar symmetric case, that is, $H \to \min$, subject to the constraints $\rho = \langle f_i \rangle$, $\rho \boldsymbol{u} = \langle f_i \boldsymbol{v}_i' \rangle$, and $\rho(DT + u^2) = \langle f_i (v_i')^2 \rangle$, where $\boldsymbol{v}_i'$ are shifted velocities.

In summary, the surprising feature of these shifted, nonsymmetric lattices is that simulations in the comoving

reference frame require no change in the LB algorithm and can be performed using the same grids as in the symmetric case. All that is needed is to replace the velocities $\boldsymbol{v}_i$ in the propagation part of the LB equation (1) with the velocities $\boldsymbol{v}_i'$ of the shifted lattice described above. This is particularly appealing for the simulation of compressible flows: The operation window of the comoving lattice Boltzmann is centered around $u = U$, in contrast to the symmetric case which operates around $u = 0$. Below, we use the entropic LB model (ELBM) introduced in Ref. [27] for the symmetric lattice (details of the algorithm can be found in Ref. [29]). Here, the ELBM [27] is realized on the shifted lattice of Fig. 1. The accuracy of the scheme was tested using the Green-Taylor vortex, and the second-order convergence pertinent to LB was confirmed also for shifted lattices.

An immediate and stark implication of the shifted lattice is seen in the following example. Figure 2 shows the pressure contours of a vortex advected by a uniform flow at three different Mach numbers, $\mathrm{Ma}_a = U_{\mathrm{in}}/\sqrt{\gamma T_{\mathrm{in}}}$, $\gamma = 1.4$ is the adiabatic exponent for air, for two different lattice configurations: the symmetric $D2Q7^2$ and its shifted version with $U = 1$ in the x direction (see Fig. 1). The vortex Mach number, employed to define the tangential velocity of the vortex, $u_\theta(r) = \mathrm{Ma}_v r \exp[(1 - r^2)/2]$, was $\mathrm{Ma}_v = 0.5$, where r is the reduced radius $r = r'/R$, and R is the vortex radius. For a vortex advected with $\mathrm{Ma}_a = 0.8$, both the symmetric and the shifted lattice give the same result. As the advection speed is increased to $\mathrm{Ma}_a = 1.3$, the standard symmetric lattice shows vortex deformation whenever the local Mach number reaches values greater than $\mathrm{Ma}_{\mathrm{loc}} > 1.6$. For the shifted lattice this does not happen, and the vortex retains its shape. By further increasing the Mach number to $\mathrm{Ma}_a = 1.8$, the standard lattice shows a completely distorted vortex while the shifted lattice operates well. Note that a majority of high Mach number flow applications, such as transonic and supersonic wings, converging-diverging nozzles, and shock-turbulence interaction, exhibit a large mean flow direction which can be readily chosen as the shift velocity. This shows a large application domain for LB in a comoving frame.

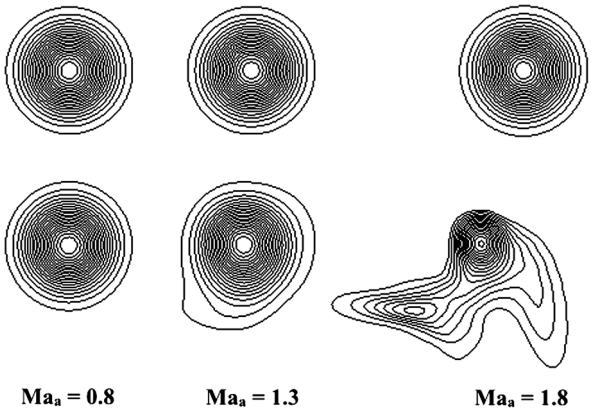

FIG. 2. Vortex advection at different Mach numbers. Top: Shifted lattice, comoving reference frame $U_x = 1$. Bottom: Symmetric lattice, standard reference frame $U_x = 0$. In the standard reference frame, the vortex is distorted at $\mathrm{Ma}_a \geq 1.3$.

In the remainder, a vortex-shock interaction is studied for the first time using the LB method. Results are benchmarked against the direct numerical simulation (DNS) of Ref. [30]. A two-dimensional vortex characterized by the Mach number $\mathrm{Ma}_v = 0.5$ is advected at the inflow Mach number $\mathrm{Ma}_a = 1.2$ and subsequently interacts with a stationary shock front (see Movie 1 in the Supplemental Material [31]). A uniform grid 1680×1440 was used in the ELBM simulation. Details on the numerical setup can be found in Ref. [30]. In Fig. 3, density ρ is compared with the DNS of Ref. [30] at the time $ta_\infty/R = 8$, where $R = 60$ is the characteristic radius of the vortex and $a_\infty = 1$ the speed of sound upstream of the shock front. One can see the deformed shock front at $x = 0$, the vortex at $x \simeq -5$ and $y \simeq 0$, and reflected shocks developing from the original planar shock, one of which remains connected to the vortex at this time. Note the excellent match of density distribution between DNS and ELBM. In Fig. 4 we compare the sound pressure $\Delta p = (p - p_s)/p_s$, where p_s is the pressure behind the shock wave. The radial sound pressure distribution in Fig. 4 was measured in the radial direction with the origin at the vortex center, at the angle $\theta = -45°$ with respect to the x axis

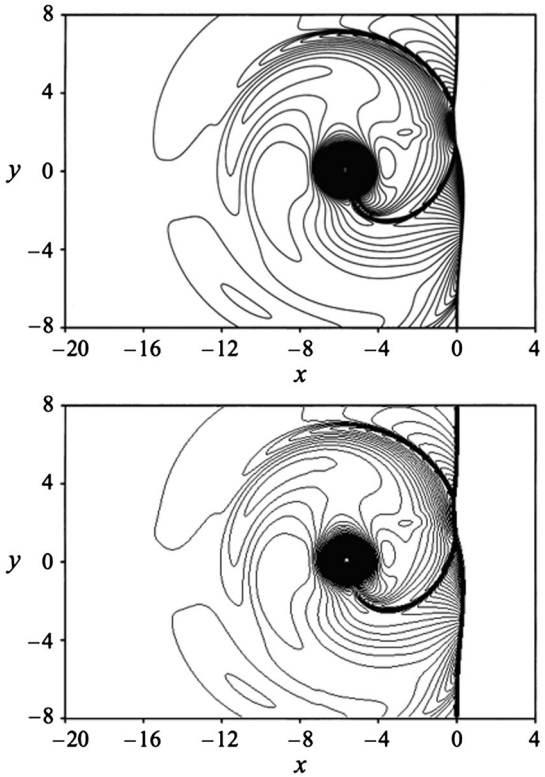

FIG. 3. Snapshot of density for both DNS (top) and ELBM simulations (bottom) for the case $\mathrm{Ma}_a = 1.2$, $\mathrm{Ma}_v = 0.5$, and $\mathrm{Re} = 400$. Contour levels are from $\rho_{\mathrm{min}} = 0.92$ to $\rho_{\mathrm{max}} = 1.55$ with an increment of $\Delta\rho = 0.0053$. The vortex moves from right to left.

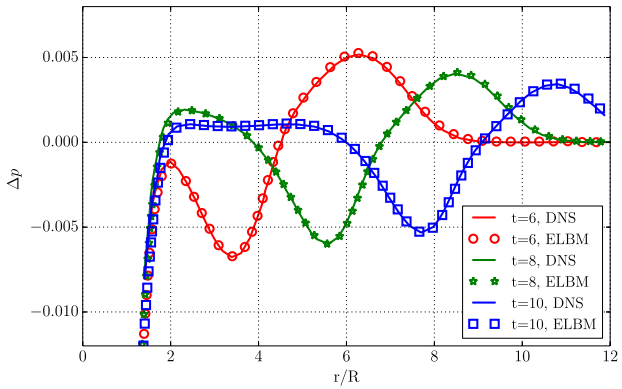

FIG. 4. Radial sound pressure distribution Δp comparison measured at an angle $\theta = -45°$ with respect to the x axis. Line: DNS [30]. Symbols: ELBM in comoving reference frame.

and at different nondimensional times $t = 6$, $t = 8$, $t = 10$. From the plot one can notice how both the sound precursor (upper sound pressure peak) and the second sound propagate radially from the vortex center with time. Moreover, the peak sound corresponding to the maximum pressure decays with time, for both the precursor and the second sound. Note that the nonlinear acoustics is typically a small (about 0.5%) perturbation on top of the main hydrodynamic pressure. The excellent comparison between the DNS [30] and the present ELBM in the comoving reference frame is evident also for this sensitive phenomenon. Finally, the present simulation is impossible with the symmetric lattice: In the laboratory reference frame, the vortex moves locally with $\mathrm{Ma}_{\mathrm{loc}} \simeq 1.7$, and is severely deformed even before it interacts with the shock (cf. Fig. 2).

To conclude, we found that the lattice Boltzmann equation is Galilean compliant. This surprising fact disproves the long-standing view on lattice kinetic theory as violating Galilean invariance by choosing the preferred reference frame "at rest." Based on that, we proposed space-filling shifted lattices which allow us to simulate in a uniform fashion the entire range of flows from incompressible to trans- and supersonic flow regimes, with no changes in the LB algorithm and no added computational cost. A benchmark simulation of vortex-shock interaction clearly demonstrates the accuracy and efficiency of the shifted lattice Boltzmann method.

This work was supported by the European Research Council (ERC) Advanced Grant No. 291094-ELBM. Computational resources at the Swiss National Super Computing Center CSCS were provided under Grants No. s492 and No. s630.

*frapolli@lav.mavt.ethz.ch
†chikatamarla@lav.mavt.ethz.ch
‡Corresponding author.
karlin@lav.mavt.ethz.ch

[1] U. Frisch, B. Hasslacher, and Y. Pomeau, Phys. Rev. Lett. **56**, 1505 (1986).
[2] G. R. McNamara and G. Zanetti, Phys. Rev. Lett. **61**, 2332 (1988).
[3] F. J. Higuera, S. Succi, and R. Benzi, Europhys. Lett. **9**, 345 (1989).
[4] Y. Qian, D. d'Humières, and P. Lallemand, Europhys. Lett. **17**, 479 (1992).
[5] S. Succi, *The Lattice-Boltzmann Equation for Fluid Dynamics and Beyond* (Oxford University Press, Oxford, 2001).
[6] H. Chen, S. Kandasamy, S. Orszag, R. Shock, S. Succi, and V. Yakhot, Science **301**, 633 (2003).
[7] M. Sbragaglia, R. Benzi, L. Biferale, S. Succi, and F. Toschi, Phys. Rev. Lett. **97**, 204503 (2006).
[8] C. Kunert and J. Harting, Phys. Rev. Lett. **99**, 176001 (2007).
[9] J. Hyvaluoma and J. Harting, Phys. Rev. Lett. **100**, 246001 (2008).
[10] L. Biferale, P. Perlekar, M. Sbragaglia, and F. Toschi, Phys. Rev. Lett. **108**, 104502 (2012).
[11] C. Antonini, S. Jung, A. Wetzel, E. Heer, P. Schoch, A. M. Moqaddam, S. S. Chikatamarla, I. Karlin, M. Marengo, and D. Poulikakos, Phys. Rev. Fluids **1**, 013903 (2016).
[12] R. Benzi, S. Chibbaro, and S. Succi, Phys. Rev. Lett. **102**, 026002 (2009).
[13] M. Mendoza, B. M. Boghosian, H. J. Herrmann, and S. Succi, Phys. Rev. Lett. **105**, 014502 (2010).
[14] M. Thiébaud, Z. Shen, J. Harting, and C. Misbah, Phys. Rev. Lett. **112**, 238304 (2014).
[15] M. Mendoza, S. Succi, and H. J. Herrmann, Phys. Rev. Lett. **113**, 096402 (2014).
[16] F. J. Alexander, S. Chen, and J. D. Sterling, Phys. Rev. E **47**, R2249 (1993).
[17] Z. Guo, C. Zheng, B. Shi, and T. S. Zhao, Phys. Rev. E **75**, 036704 (2007).
[18] X. He, S. Chen, and G. D. Doolen, J. Comput. Phys. **146**, 282 (1998).
[19] G. R. McNamara, A. L. Garcia, and B. J. Alder, J. Stat. Phys. **81**, 395 (1995).
[20] X. Shan and X. He, Phys. Rev. Lett. **80**, 65 (1998).
[21] F. Chen, A. Xu, G. Zhang, Y. Li, and S. Succi, Europhys. Lett. **90**, 54003 (2010).
[22] L. D. Landau and E. M. Lifshitz, *Fluid Mechanics* (Butterworth-Heinemann, Oxford, 1987).
[23] S. Pirozzoli, Annu. Rev. Fluid Mech. **43**, 163 (2011).
[24] J. A. Ekaterinaris, Prog. Aerosp. Sci. **41**, 192 (2005).
[25] S. S. Chikatamarla and I. V. Karlin, Phys. Rev. Lett. **97**, 190601 (2006).
[26] I. Karlin and P. Asinari, Physica (Amsterdam) **389A**, 1530 (2010).
[27] N. Frapolli, S. S. Chikatamarla, and I. V. Karlin, Phys. Rev. E **92**, 061301 (2015).
[28] I. V. Karlin, A. Ferrante, and H. C. Öttinger, Europhys. Lett. **47**, 182 (1999).
[29] N. Frapolli, S. S. Chikatamarla, and I. V. Karlin, Phys. Rev. E **93**, 063302 (2016).
[30] O. Inoue and Y. Hattori, J. Fluid Mech. **380**, 81 (1999).
[31] See Supplemental Material at http://link.aps.org/supplemental/10.1103/PhysRevLett.117.010604 for the movie of the shock-vortex interaction simulation.